ELSEVIER

Journal of Nuclear Materials 295 (2001) 97–108

journal of nuclear materials

www.elsevier.nl/locate/jnucmat

Oxidation of Zircaloy-2 and Zircaloy-4 in water and lithiated water at 360°C

M. Oskarsson [a], E. Ahlberg [b,*], K. Pettersson [a]

[a] *Department of Materials Science and Engineering, Royal Institute of Technology, SE 10044 Stockholm, Sweden*
[b] *Department of Chemistry, Göteborg University, SE 41296 Göteborg, Sweden*

Received 15 October 2000; accepted 8 January 2001

Abstract

Zircaloy-2 and Zircaloy-4 samples were oxidised in an autoclave in water and in lithiated water (70 ppm) in order to evaluate the influence of both the alloy compositions and the effect of lithium on the oxidation kinetics. Cross-sectional TEM and electrochemical impedance spectroscopy were used to analyse the samples. The pre-transition oxidation rate is not affected by the presence of LiOH, but the transition occurs earlier and the post-transition oxidation rate is increased. The oxidation rate correlates with the density of cracks in the oxide layer and the morphology of the oxide grains. The impedance measurements show that the oxides formed have a layered structure and for samples oxidised in LiOH solution the inner protective layer is thin. The hydrogen pickup ratio follows the weight gain, not the oxidation rate, up to the second transition. When the protective oxide layer is degraded the hydrogen pickup ratio increases strongly. The effect of LiOH is suggested to be due to partial dissolution of the oxide and subsequent incorporation of lithium ions during a dissolution–precipitation process. Newly formed oxide is probably more hydrous and the grain boundaries are particularly liable to dissolution. The up-concentration of LiOH within cracks and pores could cause the detrimental levels necessary for dissolution. This is supported by the insensitivity in the pre-transition region, to both the compositions of the alloy and to the environment.

1. Introduction

Lithium is added to the primary water in pressurised water reactors (PWR) to control the pH value and thereby the corrosion of structural materials. The pH value is recommended to be between 7.2 and 7.4, but local boiling at the fuel rod surface leads to enrichment of lithium hydroxide and detrimental levels may be reached.

Different mechanisms describing the accelerated oxidation in the presence of lithium have been discussed in the literature. One proposed mechanism by which LiOH increases the corrosion rate is by substitutional solid solution of lithium in the oxide layer [1]. When one Zr^{4+} ion is replaced with Li^+ in the ZrO_2 lattice one and a half anion vacancies are created. An increase in the anion vacancy concentration will enhance the oxygen diffusion through the oxide layer. Cation incorporation into ZrO_2 has also been suggested to control the oxide microstructure, the oxide growth mechanism at the metal–oxide interface and the corrosion rate [2]. Corrosion tests of Zircaloy-4 in various aqueous solutions with equimolar M^+ (Cs^+, Rb^+, K^+, Na^+ and Li^+) and OH^- at 350°C showed that the corrosion rate is significantly accelerated in LiOH and slightly enhanced in NaOH, but no acceleration was observed in the other solutions. The hydrogen pickup fraction has a similar trend as the corrosion behaviour in different solutions [2]. In another model the generation of porosity rather than the dissolution of lithium in the growing oxide phases was proposed to cause the accelerated corrosion [3]. It is suggested that undissociated LiOH and hydroxyl ions react at an anion vacancy and form Zr–OLi groups. The recrystallisation and oxide growth is disturbed by the presence of these Zr–OLi groups and a larger grain boundary area may be expected. Two Zr–OLi groups could also react with each other and form

* Corresponding author. Tel.: +46-31 772 2879; fax: +46-31 772 2853.
E-mail address: ela@inoc.chalmers.se (E. Ahlberg).

0022-3115/01/$ - see front matter
PII: S0022-3115(01)00480-9

Li_2O in the grain boundary, generating porosity in the growing oxide. Porosity has also been proposed to be generated by preferential dissolution of cubic or tetragonal crystallites in the oxide [4,5]. The effect of LiOH has been reported to be twofold: (i) reducing the time to transition and (ii) enhancing the post-transition rate [6]. Lithium hydroxide is suggested to enhance the oxidation by degrading the barrier layer. For the post-transition corrosion it has been proposed that the corrosion process proceeds within cracks in the oxide film [7]. The rate is accelerated due to an accumulation of LiOH within the cracks, since the corrosion process consumes water and the circulation is restricted.

In this work, both Zircaloy-2 and Zircaloy-4 have been oxidised in a refreshed autoclave and the environments were pure water or water with 70 ppm lithium hydroxide added. Zircaloy-2 is normally used in boiling water reactors (BWR) but has also, in Sweden, been tested in PWR environment. The oxide layer formed was characterised by cross-sectional transmission electron microscope (TEM) and electrochemical impedance spectroscopy (EIS) with the purpose of improving our understanding of the mechanism by which lithium influences the oxidation and hydriding of Zircaloy.

2. Materials

The materials investigated are two Zircaloy-2 alloys and one Zircaloy-4 alloy. Sandvik Steel AB manufactured the materials as tubes. Material Zry-4:A is a Zircaloy-4 alloy and the chemical composition is given in Table 1, together with the $\log A$ parameter for all samples. In Zircaloy-4 only the $Zr(Fe,Cr)_2$ second-phase particles are formed and for Zry-4:A the mean diameter is 160 nm. Material Zry-2:A and Zry-2:B are Zircaloy-2 alloys with the chemical composition given in Table 1. The Zry-2:B alloy has a higher tin content, but a lower content of elements forming second-phase particles than alloy Zry-2:A. Further, the Zry-2:B has a late β-quenching step, yielding small second-phase particles (mean diameter 80 nm). For Zry-2:A the second-phase particles are larger with a mean diameter of 240 nm. These two materials were chosen on the basis of earlier autoclave tests, having good (Zry-2:B) and bad (Zry-2:A) corrosion resistance in lithiated environment, respectively.

3. Experimental

The materials were oxidised in a refreshed autoclave at 360°C and 220 bar, in pure water or in water with addition of 70 ppm Li. The samples were degreased before the oxidation.

To characterise the microstructure of the oxide layers a JEOL 2000 EX scanning transmission electron microscope was used. Cross-sectional thin foils of the oxide layers were produced from the autoclaved samples and the detailed procedure is given elsewhere [8]. Samples with thicker oxide layer (>10 μm) were rather time-consuming to produce, since the oxide had a strong tendency to fall off during the last thinning step. Several thin foils were prepared for each sample to guarantee the reproducibility.

A three-electrode cell was used for the impedance experiments in aqueous 0.5 M Na_2SO_4. 1 cm of the autoclaved Zircaloy tubes were used as working electrodes in the impedance measurements. The contacting was made on the inside of the tube and epoxy resin was used to isolate the contact and bare metal ends from the electrolyte. A large platinum gauze was used as the counter electrode and was placed in a concentric position around the working electrode to assure a good current distribution. The potential was measured against a double junction Ag/AgCl reference electrode with 0.5 M Na_2SO_4 in the outer compartment. The electrolyte was made up by p.a. quality chemicals and doubly distilled water. All impedance measurements were carried out at room temperature, in the frequency range 1 mHz to 100 kHz. The instrumentation used was an EG&G Princeton Applied Research Potentiostat/Galvanostat Model 273A, and a Schlumberger SI 1255 HF frequency response analyser.

The impedance data were fitted to equivalent circuits with one, two or three time constants in series, using Boukamp's fitting program 'Equivalent circuit'. The number of time constants used depends on the complexity of the impedance spectra.

Table 1
Chemical composition of the materials

Material	Sn (%)	Fe (%)	Cr (%)	Ni (%)	O (%)	
Zry-4:A	1.33	0.215	0.10	0.002	0.120	
Zry-2:A	1.34	0.17	0.10	0.05	0.126	
Zry-2:B	1.48	0.125	0.08	0.045	0.103	
	Si (ppm)	N (ppm)	H (ppm)	C (ppm)	Alloy	$\log A$
Zry-4:A	75	$\leqslant 30$	9	140	Zr-4	−12.9
Zry-2:A	70	$\leqslant 33$	11	135	Zr-2	−5.8
Zry-2:B	80	$\leqslant 30$	10	110	Zr-2	−16.0

Zirconium oxide is highly insulating and the overall impedance can therefore be attributed to the impedance of the oxide. The oxide behaves like a capacitor in the impedance measurements and the thickness can be calculated by the expression for a parallel plate capacitor,

$$d = \frac{\varepsilon_0 \varepsilon_r A}{C}, \quad (1)$$

where ε_0 is the dielectric constant of vacuum, ε_r the relative dielectric constant for ZrO_2, A is the geometric surface area, d is the thickness of the oxide layer and C is the capacitance. The impedance data exhibit some frequency dispersion and a constant phase element was used instead of a capacitor. Due to the frequency dispersion the capacitance, and thereby the thickness will vary with frequency. Two strategies were used to compare data from different measurements. Firstly, to estimate the total thickness of the oxide layer the capacitance value at 60 kHz was used. Secondly, the capacitance value obtained in the fitting procedure was used to estimate the apparent thickness of the different layers of the oxide. The capacitance value was not corrected for the frequency dispersion but the calculated thickness data were scaled to the value obtained from the thickness determined at 60 kHz.

4. Results

The weight gain during oxidation for the different materials is given in Fig. 1. The presence of LiOH seems to have little effect on the pre-transition oxidation rate. However, the transition from parabolic/cubic to linear growth rate occurs earlier in lithiated water than in water and the post-transition oxidation rate is increased. The Zircaloy-4 sample Zry-4:A has a somewhat higher oxidation rate than Zircaloy-2, during tests in lithiated water. However, the second transition appears later and the acceleration in corrosion rate is lower. Sample Zry-2:A, tested in water, has the slowest oxidation rate in the post-transition region. The linear growth rate indicates that the rate is limited by diffusion of oxygen ions through a fairly constant oxide layer thickness. In the lithiated water, the Zry-2:A alloy has the lowest corrosion resistance of all tested samples. The post-transition region is very limited, and the second transition occurs very early resulting in accelerated oxidation kinetics. The increasing oxidation rate indicates that the barrier layer thickness is decreasing. The other Zircaloy-2 sample (Zry-2:B) has a better corrosion resistance in lithiated water and the post-transition oxidation is in parity with the oxidation in water for the other two alloys. At about 130 days the second transition occurs and the accelerated oxidation rate starts.

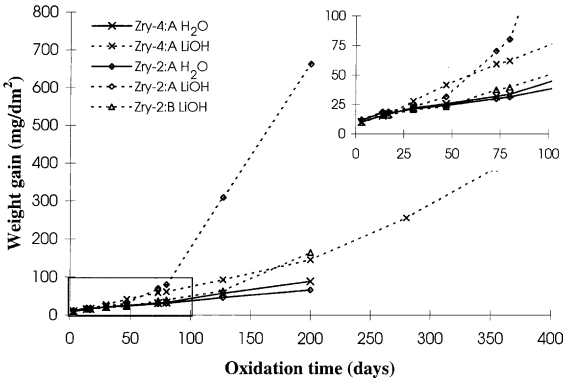

Fig. 1. Corrosion kinetics for the studied materials. Autoclaved at 360°C and 220 bar, in pure water or in water with addition of 70 ppm Li.

The hydrogen pickup was measured for some of the oxidised samples and the result is given in Table 2. As expected, the Zircaloy-4 sample has the lowest pickup ratio both in water and in lithiated water. For long time exposure, i.e., after the second transition, the hydrogen pickup ratio has increased by a factor of 2.5. For

Table 2
Oxide thickness and hydrogen pickup as a function of alloy composition, environment and exposure time

Material	Environment	Time (days)	Weight gain (mg/dm^2)	Oxide thickness (μm)[a]	H pickup (ppm)	H pickup ratio (%)
Zry-4:A	H_2O	30	22.1	1.5	–	–
Zry-4:A	70 ppm Li	30	27.9	1.9	–	–
Zry-4:A	H_2O	200	89.3	5.9	120	20
Zry-4:A	70 ppm Li	73	59.2	3.9	72	18
Zry-4:A	70 ppm Li	353	386.6	25.8	1200	47
Zry-2:A	H_2O	30	21.2	1.4	–	–
Zry-2:A	70 ppm Li	30	23.3	1.6	–	–
Zry-2:A	H_2O	200	67.1	4.5	170	38
Zry-2:A	70 ppm Li	200	663.6	44.2	2750	62
Zry-2:A	70 ppm Li	73	70.3	4.7	170	43
Zry-2:B	70 ppm Li	200	164.9	10.9	640	64

[a] Thickness calculated from weight gain (15 mg/dm^2 $\sim$ 1 μm).

Zry-2:A a small difference in the pickup ratio can be noted by comparing the oxidation in water (200 days) with that in lithiated water (73 days) at a similar weight gain. Oxidation of Zry-2:A and Zry-2:B in lithiated water for 200 days results in similar pickup ratios despite the big difference in weight gain.

4.1. TEM investigation

Samples for the cross-sectional TEM investigation were chosen in such a way that both the alloy composition and the effect of lithium on the oxidation kinetics were highlighted. The 30 days samples with similar weight gain illustrate the non-sensitivity to both the environment and the alloy composition. Comparing samples subjected to the same oxidation time and the same environment can outline the effect of different alloy compositions. Using one alloy and comparing samples with similar weight gain, the influence of the environment can be depicted.

The TEM investigation was focussed on the oxide and the oxide–metal interface. Columnar grains were mainly found in the oxide close to the interface and this region seems to be dense and compact. It is sometimes referred to as the barrier layer, where the environment does not penetrate the oxide. Outside this region, a mixture of equiaxed and columnar oxide grains are observed. The fraction of grain type depends on the oxidation time and the environment. In this work an oxide grain is defined as columnar when the length is more than twice the width. The growth of the columnar grains is perpendicular to the oxide–metal interface.

Cracks were found in the studied oxide layers and were mainly oriented parallel with the interface. The cracks in the oxide layer may originate both from the oxidation process and from the metallographic sample preparation technique [9]. Large compressive stresses present in the oxide film will be released when the thin TEM samples are prepared and cracks could be expected, but it is difficult to separate cracks present before preparation and those formed during preparation. The oxide grains are mainly equiaxed around the cracks. The reason for this may be due to (i) crack propagation through columnar grains, causing morphological changes,

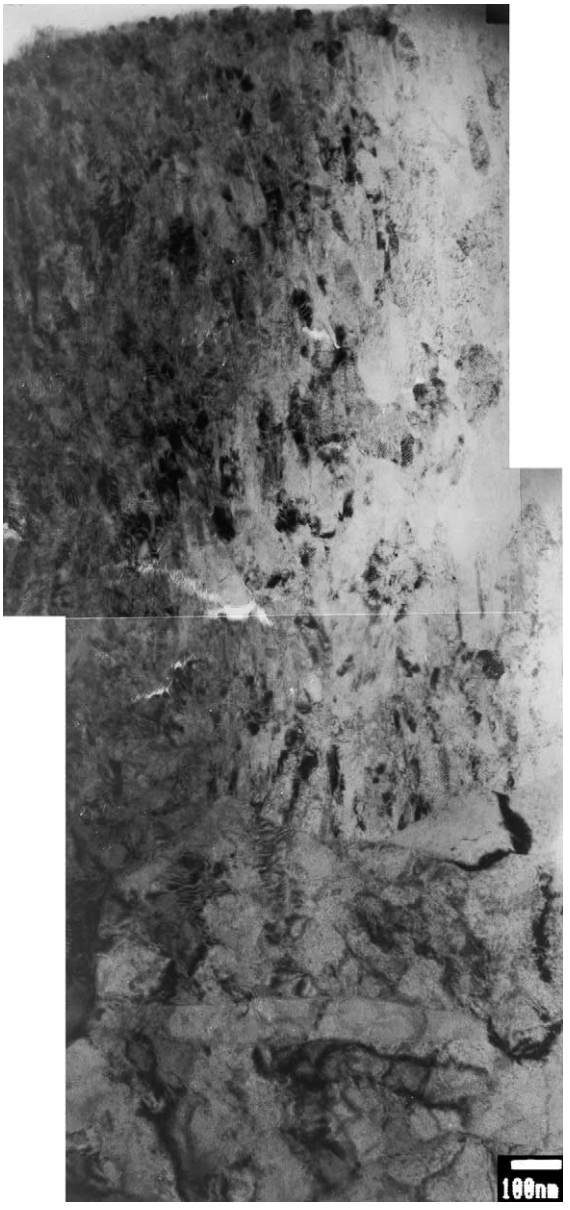

Fig. 2. Sample Zry-4:A after oxidation for 30 days in water. The entire oxide layer is imaged.

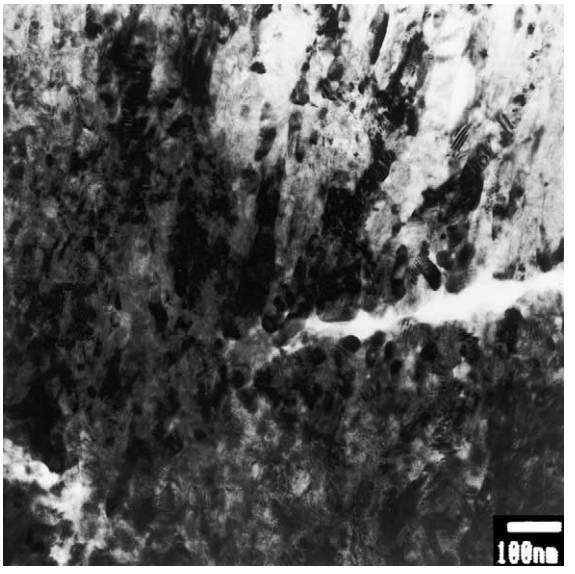

Fig. 3. Sample Zry-4:A after oxidation for 73 days in lithiated water. The middle section of the oxide layer is imaged.

(ii) preferential crack propagation in equiaxed areas and (iii) nucleation of equiaxed grains at crack formed closed to the metal–oxide interface during the oxidation process.

The Zircaloy-4 sample Zry-4:A, autoclaved 30 days in pure water, has an oxide structure of columnar grains close to the interface and also in the middle section there is mainly columnar oxide grains, see Fig. 2. Cracks parallel to the interface are found in this region. The sample tested for 30 days in lithiated water, has a similar microstructure. The oxide grain size was estimated to be 20–40 × 70–200 nm^2 (columnar) and a diameter of 20–40 nm (equiaxed), respectively. After 200 days in pure water the oxide at the interface still contains columnar grains. Outside this region, a small fraction of equiaxed grains is mainly found at cracks present. Sample Zry-4:A autoclaved for 73 days in lithiated water, see Fig. 3, has a morphology similar to the sample Zry-4:A tested for 200 days in pure water. However, the fraction of equiaxed oxide grains is slightly higher for the former sample. The hydrogen pickup ratio is similar, despite the 50% difference in weight gain, see Table 2. For the Zircaloy-4 the hydrogen absorption was smaller than for the two other tested materials. Nickel is believed to be responsible for the higher hydrogen pickup in Zircaloy-2 [10].

The Zry-2:A alloy had poor corrosion resistance in lithiated water. After tests at 30 days in pure water and

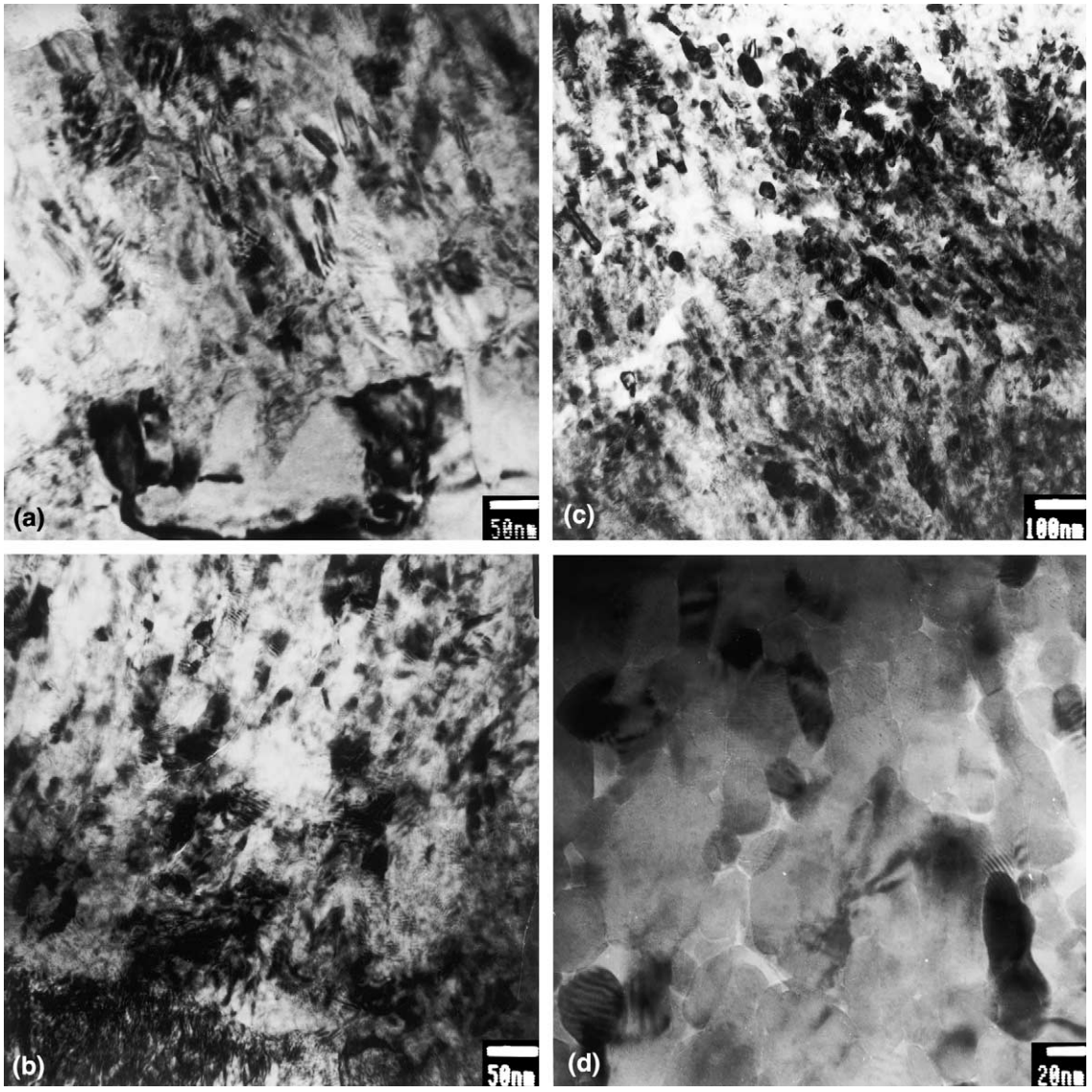

Fig. 4. Sample Zry-2:A after oxidation for 200 days: (a) in water, the metal–oxide interface; (b) in lithiated water, the metal–oxide interface; (c) in lithiated water, middle section of oxide layer; (d) in lithiated water, outer section of oxide layer.

lithiated water the oxide layer at the interface consists of columnar oxide grains. In the outer part equiaxed grains develop. The weight gain is similar for these two samples and no difference in morphology was detected. The grain size for alloy Zry-2:A is in parity with the investigated Zircaloy-4 samples.

Sample Zry-2:A autoclaved for 200 days in pure water and lithiated water has major differences in morphology and weight gain. For the sample tested in water a morphology of columnar oxide grains is observed at the interface. Outside this area, there is a majority of columnar grains, but equiaxed grains are also present, Fig. 4(a). Compared to the sample after 30 days testing, the oxide layer is thicker and the morphology outside the interface region has more equiaxed grains present, probably due to the presence of more cracks. The sample tested in lithiated water has a mixture of columnar and equiaxed grains at the interface, as shown in Fig. 4(b), and the interface region is thinner. The middle section of the oxide layer has more cracks and an increased fraction of equiaxed oxide grains as shown in Fig. 4(c). The outer oxide is rather porous and an example of a non-protective oxide is shown in Fig. 4(d). The size of the columnar grains was found to be smaller, approximately $20–30 \times 60–100\ nm^2$ and the oxide layer has many cracks and open porosity was also found. The hydrogen content is extremely high in this sample, see Table 2.

Sample Zry-2:A, autoclaved for 73 days in lithiated water, has a similar weight gain to the sample tested for 200 days in water. The morphology at the interface is the same with mainly columnar oxide grains. In the outer region of the oxide a larger number of equiaxed grains and more cracks were found in the sample exposed to lithiated water. The hydrogen content is similar for these two samples, but the pickup ratio is slightly larger for the sample oxidised in the presence of lithium, see Table 2.

The high Sn Zircaloy-2 sample (Zry-2:B) exhibits a lower weight gain when oxidised for 200 days in lithiated water than Zry-2:A. At the interface columnar grains are present, while outside this area a mixture of columnar and equiaxed grains is found, see Fig. 5. Compared to the sample Zry-2:A, oxidised under the same conditions, the outer oxide layer is much denser and a higher fraction of columnar oxide grains is retained. However, some porosity was found in the outer oxide. The grain size in the oxide is of the same size as for sample Zry-2:A. Surprisingly, the hydrogen pickup ratio was similar for the two materials, despite the large difference in the oxidation rate.

4.2. EIS measurements

Impedance measurements can provide information about the porosity of the oxide and its homogeneity. If a dense oxide is formed, one time constant is sufficient to model the impedance data. The frequency dispersion commonly observed, can in this case be attributed to surface roughness of the underlying metal and dielectric relaxation [11–13]. If the oxide is composed of layers with different properties several time constants are needed to model the data. The change in properties can originate from a difference in the dielectric properties or from changes in the pore structure. Large differences in the dielectric constant for ZrO_2 on zirconium and zirconium alloys have been reported, between 21.4 and 31.5 [14,15] and have, for example, been attributed to anion incorporation in anodically formed oxides. In the present investigation a value of 22 was used for the relative dielectric constant of ZrO_2.

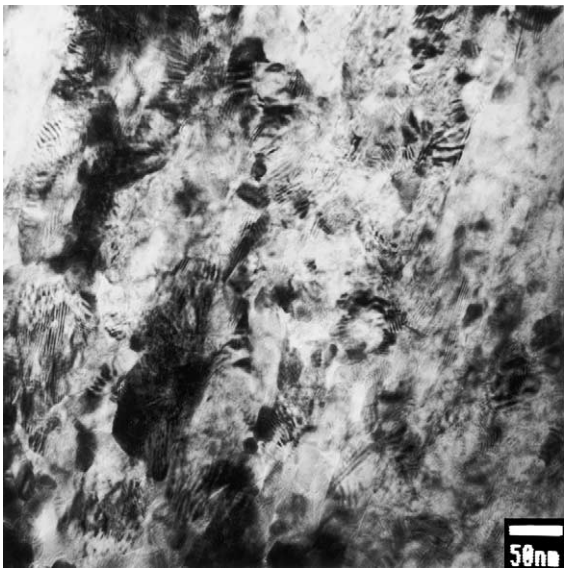

Fig. 5. Sample Zry-2:B after oxidation for 200 days in lithiated water. The middle section of the oxide layer is imaged.

Impedance measurements on the autoclaved samples were made as a function of time to follow the penetration of the electrolyte into the pores. These measurements will give a qualitative picture of the properties of the oxide. In Fig. 6 impedance spectra for sample Zry-4:A exposed to water at 360°C for 200 days and to lithiated water for 73 days are shown. For the sample exposed to water, Fig. 6(a), initially only one time constant can be observed (curve 1), but the frequency dispersion is quite large, indicating that the oxide is inhomogeneous. For longer exposure times electrolyte has penetrated into the oxide, the resistance is markedly decreased and two time constants are necessary to model the data (curves 2 and 3). The electrolyte is supposed to get in contact with conducting paths in the oxide, consisting of pores running all the way to the metal interface, metal strings in the oxide or a defect oxide with higher conductivity than monoclinic ZrO_2, causing the dramatic decrease in the resistance. At very long exposure times the inner part of the oxide is changed and a new time constant is visible in the impedance spectra

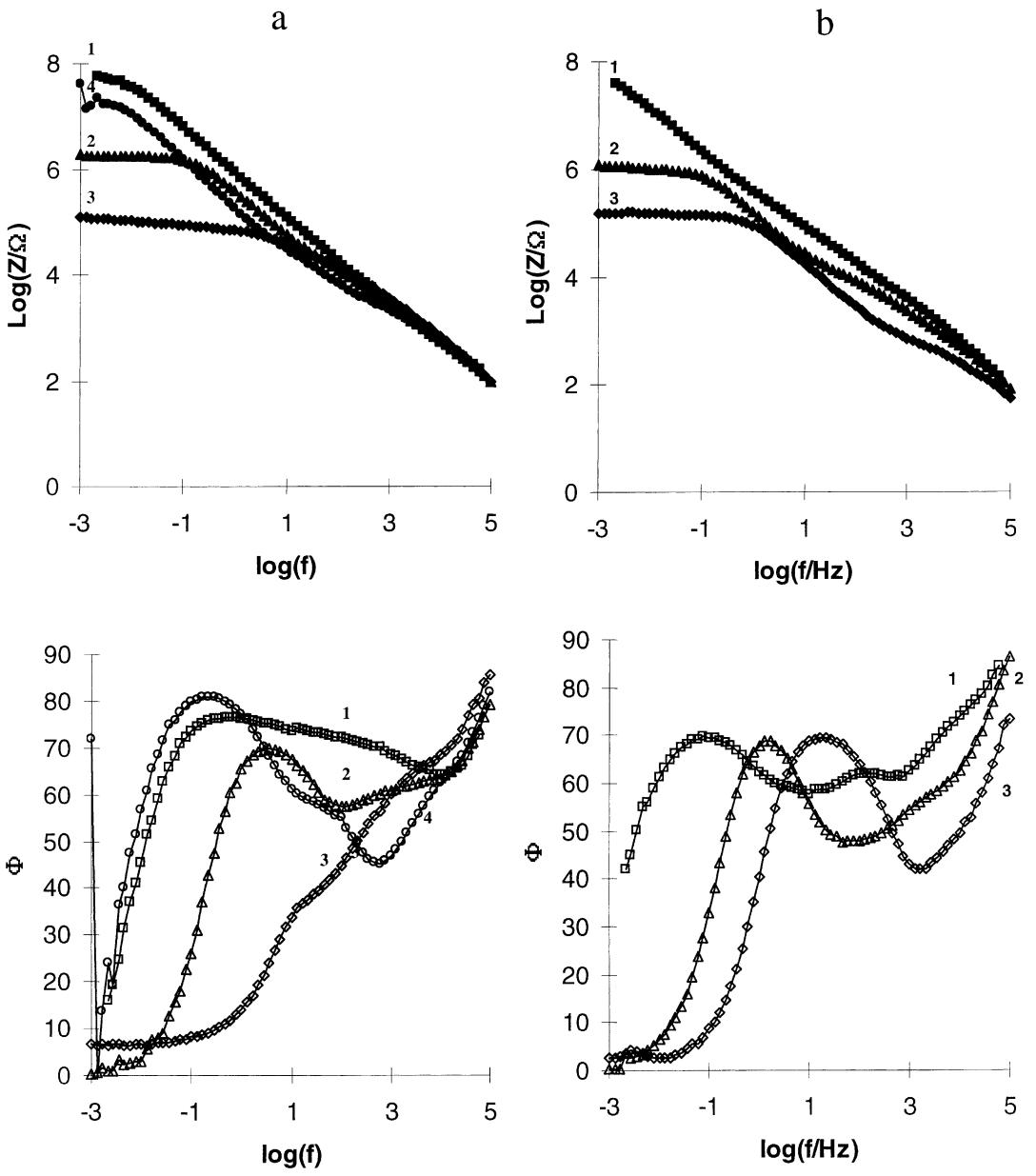

Fig. 6. Impedance spectra for sample Zry-4:A as a function of immersion time: (a) exposed 200 days in water for 19 h (1), 360 h (2) 1500 h (3) and 3600 h (4); (b) exposed 73 days in lithiated water for 15 h (1), 330 h (2) and 1500 h (3).

(curve 4). The inner part of the oxide is thus healed either by a transformation of the conducting oxide or by an oxidation of the metal strings. For the sample exposed to lithiated water, Fig. 6(b), three time constants are seen from the start (curve 1) and the electrolyte can readily penetrate the oxide. The oxide thickness was calculated from the capacitance at 60 kHz and decreases as a function of the exposure time in the electrolyte. The thickness obtained directly on immersion of the samples correlate very well with the values calculated from the weight gain, see Table 2. A comparison of the oxide thickness for sample Zry-4:A in the different environments is shown in Fig. 7. For the sample exposed to lithiated water, the thickness obtained for the well soaked sample was only 0.5 μm as compared to the real oxide thickness of 3.5 μm. The fact that the apparent oxide thickness decreases is due to a decreasing resistance over the oxide as a result of the electrolyte penetration, since the low resistance together with a small capacitance will yield a time constant that falls outside

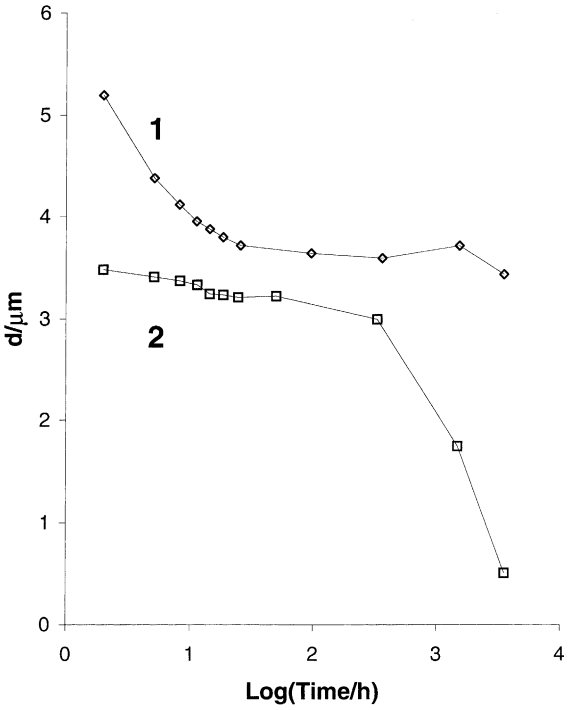

Fig. 7. Oxide thickness determined by EIS as a function of immersion time for sample Zry-4:A. Sample oxidised in water for 200 days (1) and in lithiated water for 73 days (2).

the accessible frequency range. These results show that the porosity of the oxide film gradually decreases from the oxide–solution interface to the metal–oxide interface. A model with three or sometimes four layers is therefore proposed. The inner layer at the metal–oxide interface (I) is compact and impervious to the electrolyte. The middle range (II), which can be composed of different layers, is microporous, allowing for limited penetration of electrolyte, while the outer layer is macroporous (III). The outermost layer is not discernible by impedance measurements since the time constant falls outside the accessible frequency range.

The impedance characteristics for the other samples follow the same general features. For the Zry-2:A sample exposed to water for 200 days, two time constants were observed throughout the exposure time (up to 3700 h) The capacitance at high frequencies remains constant with time, indicating that the oxide is fairly dense. The thickness calculated from the impedance at 60 kHz is in good agreement with the thickness calculated from the weight gain, Table 2. The resistance of the film decreases initially with one order of magnitude, but after long exposure time the resistance is again higher. When exposed to lithiated water for the same exposure time (200 days) three time constants are present from the beginning of exposure. The resistance of the oxide decreases by two orders of magnitudes and the time constant for the innermost layer disappears with time. The oxide thickness as determined by impedance was 17 μm, which is much thinner than predicted from the weight gain, Table 2. Thus, it can be concluded from the impedance measurements that the major part of the oxide is macroporous and thus not discernible by impedance measurements. The oxide formed on sample Zry-2:A exposed to lithiated water for a shorter exposure time (73 days) is compact and only one time constant is observed initially. However, the resistance of the oxide decreases dramatically with time and a second time constant starts to evolve. After long exposure times the total oxide resistance is again high, which indicates that the pores in the oxide has partly disappeared. The thickness of the layer is in good agreement with the weight gain predictions. For sample Zry-2:B exposed to lithiated water for 200 days the oxide thickness determined by impedance is in fairly good agreement with that predicted from the weight gain, indicating a fairly compact oxide layer. However, already from the initial exposure, three time constants can be observed in the impedance spectra. As for the other samples the resistance of the oxide decreases with time, but the capacitance at high frequencies remains constant.

In Table 3 a summary of the impedance results for well soaked samples are given according to the multi-

Table 3
Oxide thickness calculated by EIS

Material	Environment	Time (days)	Thickness (μm)[a]	I (nm)[b]	II (μm)[c]	II (μm)	III (μm)[d]
Zry-4:A	H_2O	200	5.9/5.2	800	2.6		2–2.5
Zry-4:A	70 ppm Li	73	3.9/3.5	170	0.33		3–3.4
Zry-2:A	H_2O	200	4.5/3.8	1000	2.5		0.3–1
Zry-2:A	70 ppm Li	200	44.2/17.1	30	1.6	11	30
Zry-2:A	70 ppm Li	73	4.7/4.5	40	4.5		0.2
Zry-2:B	70 ppm Li	200	10.9/8.8	30	0.9	6.3	1.6–3.6

[a] Thickness calculated from weight gain (15 mg/dm^2 $\sim$ 1 μm)/thickness calculated from EIS.
[b] Barrier layer.
[c] Microporous layer.
[d] Outer macroporous layer.

layer model. The thicknesses of the inner layers are calculated from the circuit parameters obtained by the fitting procedure and scaled to the total thickness determined at 60 kHz. The thickness of the macroporous layer is simply the difference between the total thickness and the sum of the thickness for the inner layers. In general the thickness determined by impedance measurements is in good agreement with the thickness obtained from the weight gain, except for the thickest oxide where only a part of the oxide can be detected by impedance. However, the pore structure of the oxides differs. For samples exposed to lithiated water, the inner layer is always thin and the middle layer can sometimes be divided into two layers. In contrast, for the samples exposed to pure water the inner layer is rather thick ($\sim$1 μm).

The multi-layer observed with impedance measurements can be compared with the two layers found in the TEM investigation, the inner dense layer and the outer layer with visible cracks. Only for the sample Zry-2:A oxidised in lithium for 200 days a change of the inner layer was observed in TEM. The high oxidation rate for this sample explains the changed morphology.

5. Discussion

This investigation showed that the morphology of the formed oxide in presence of lithium hydroxide is disturbed compared to oxidation in pure water. A higher fraction of equiaxed grains is found outside the barrier layer and the oxide formed during accelerated corrosion has less columnar grains. Open porosity was found in areas with equiaxed grains, Fig. 4(d), in the outer part of the oxide and can be correlated with the macroporous layer found in the impedance measurements. The barrier layer thickness decreases when the accelerated oxidation starts, and the morphology of the inner layer changes from columnar to a mixture of columnar and equiaxed grains. A decrease in thickness of the barrier layer at longer exposure times in lithiated environment has been reported elsewhere [6,16] and is also in agreement with our impedance data. The effect of lithium on the corrosion behaviour of Zircaloy has received great attention during the years and different hypotheses have been put forward to explain the results. Common to the different models and hypotheses is the distinct influence of lithium on the oxide microstructure [3–6,9,16–20].

The corrosion rate for zirconium alloys is well known to increase with increasing pH. However, the effect obtained in LiOH solutions is much stronger than in NaOH or KOH solutions, and therefore lithium rather than hydroxide ions was considered to be the main cause of the accelerated corrosion rate [1,2,7,17,19,21]. Corrosion tests were performed in lithium salts but no effect was found on the oxidation rate, ruling out the lithium ion as the only species causing accelerated corrosion [1]. The lithium hydroxide concentration must be above a critical level to accelerate the corrosion rate [21,22] and it has been suggested that the active species is undissociated LiOH [3,5,18]. The large effect of temperature also supports the importance of undissociated LiOH, since its concentration increases with increasing temperature [23].

In the model by Cox et al. [4,5,20] the accelerated corrosion is explained by preferential dissolution of oxide grains with cubic or tetragonal crystal structure, leading to a porous inner oxide layer. To support this hypothesis microscopic investigations were made on a pre-oxidised sample that was subjected to 0.1 M LiOH solution. It was found that a number of pores were developed on the outer oxide surface. Further, the importance of preferential dissolution of the tetragonal modification was emphasised by referring to an investigation where Yttria stabilised Zirconia (YSZ) was tested in water and alkali solutions at 600–780°C and 100 MPa [24]. The YSZ was unchanged in water while it was reported to dissolve (and precipitate as monoclinic oxide) in alkaline solutions, in the order LiOH > NaOH > KOH. However, corrosion tests on stabilised zirconia do not support the model with preferential dissolution [25]. These corrosion tests were performed under conditions similar to autoclave testing of Zircaloy, i.e., 400°C and 10 MPa. The tests were performed in pure water or 1.0 M LiOH solution for 3 days in a mini autoclave. Different types of stabilised zirconia were tested, including both yttrium and size stabilised, both yielding the tetragonal modification. A phase transformation from tetragonal to monoclinic oxide was detected by X-ray diffraction after the test. No difference in the phase transformation rate was detected between the two environments. However, the YSZ was found to have a higher transformation rate than the size stabilised oxide [25].

For pre-transition oxidation in water (288–360°C) of Zircaloy-2 and Zircaloy-4, only very small amounts of tetragonal zirconium oxide was detected by X-ray diffraction [26] as shown for a standard Zircaloy-4 in Fig. 8. This implies that the porous structure of the oxide formed in lithium hydroxide solution [4] is not entirely due to preferential dissolution of the tetragonal modification, but may well be due to partial dissolution of the oxide. Newly formed oxide is probably more hydrous [27] and it is reasonable to assume that the grain boundaries are particularly liable to dissolution, which can explain the formation of the small pores. The upconcentration of LiOH within cracks and pores could cause the detrimental levels necessary for dissolution.

A metal oxide exposed to water will exhibit acid–base properties. The surface hydroxide groups are amphoteric and can therefore be protonated and deprotonated. Thus, in alkaline solution the surface will be negative

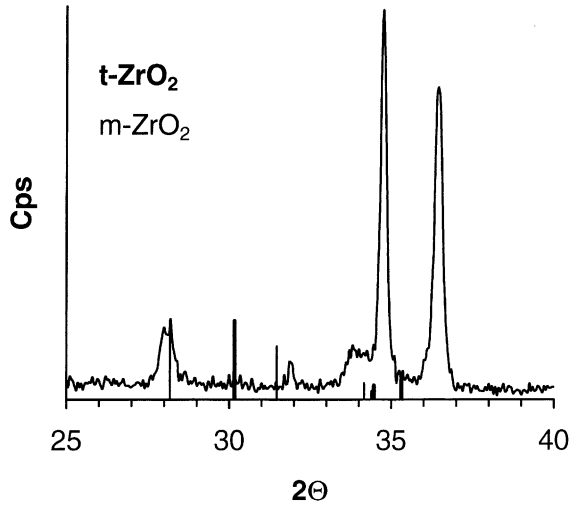

Fig. 8. Grazing angle X-ray diffraction of standard Zry-4, oxidised in water for 4 days at 360°C and 186 bar. The reflections at 30.2, 34.8 and 36.5 2Θ originate from α-Zr.

and the surface charge is balanced by cations in solution. Interfacial properties of zirconium dioxide have been studied at room temperature by measurements of the electrophoretic mobilities and surface charge densities [28]. The results have been discussed in terms of a site binding model, in which the contribution to the generation of surface charge from the indifferent electrolyte ions is stressed [29–33]. In the model the formation of ion pairs between the surface groups and the electrolyte ions were proposed,

$$\equiv\mathrm{SOH}^{\circ} + \mathrm{X}^{-} + \mathrm{H}_{s}^{+} \leftrightarrow \equiv\mathrm{SOH}_{2}^{+} - \mathrm{X}^{-} \quad K_{\mathrm{anion}}$$
$$\equiv\mathrm{SOH}^{\circ} + \mathrm{M}^{+} \leftrightarrow \equiv \mathrm{SO}^{-} - \mathrm{M}^{+} + \mathrm{H}_{s}^{+} \quad K_{\mathrm{cation}},$$

where $\equiv$S denotes a surface site and MX is the indifferent electrolyte salt. Measurements were made as a function of electrolyte concentration and rather strong site binding with surface hydroxide groups was found. The pH of zero charge for zirconium dioxide was determined to be 6.4, taking into account the influence of electrolyte ion adsorption. A specific adsorption of electrolyte cations is commonly found for oxides [34].

Thus, in the alkaline environment in the pores of the oxide, the surface will be highly negatively charged and lithium ions will be strongly bound to the oxide surface. The presence of lithium ions on the oxide surface can result in both an incorporation of Li^+ in the oxide by a dissolution–precipitation reaction and by an effect on the crystallisation rate.

It has been observed that high oxidation rates result in formation of equiaxed grains [6,16,17]. But smaller grains can also be formed by precipitation of zirconium oxide in the presence of cations, favouring the tetragonal modification [35]. By contacting hydrous zirconium oxide with Na^+ solution at a given pH it could be shown that sodium ions are adsorbed on the hydrous zirconium oxide in different amounts depending on the pH value. Adsorbed sodium ions slow down the crystallisation process and sodium will be present in different locations, as atomically dispersed on the surface, as Na_2O crystals and incorporated in solid solution. The amount of sodium that is incorporated depends on the pH of solution and temperature, but is always less than 1 wt% [35]. However, lithium ions have comparable size to Zr^{4+} and it can be expected that a larger number of lithium ions can be found in solid solution. In fact, when the accelerated corrosion occurs and the barrier layer has degraded, a high concentration of lithium can be found at the oxide–metal interface, as determined by SIMS analysis [6,16]. Both the oxidation rate and the presence of cations may therefore contribute to the appearance of equiaxed grains. If lithium should have any effect on the diffusion of hydrogen and oxygen through the inner protective layer, it must be incorporated in the oxide. The incorporation of lithium may take place under circumstances where a dissolution–precipitation process occurs. This is consistent with the oxidation kinetics being independent of both the compositions of the alloy and the environment, in the pre-transition region. SIMS profiling show very low amounts of lithium in the barrier layer (<20 ppm) [6,16]. In the pores, where the concentration of lithium hydroxide increases with time, due to the restricted exchange with the bulk solution, partial dissolution can take place. The dissolution reaction consumes hydroxide ions and the oxide is again precipitated possibly incorporating some lithium in solid solution. This will increase the anion vacancy concentration at the surface of the pores and further increase the diffusion of oxygen.

The rate controlling process in Zircaloy oxidation is the transport of oxygen across the dense inner layer of the oxide. In the post-transition region the oxidation kinetics are linear, implying that the thickness of the inner layer is constant. The oxygen transport through the oxide layer is believed to proceed by grain boundary diffusion. It has been proposed that the width of the grain boundaries may be affected by the pH value, such that the width is increased with increasing pH [19]. An enlargement of the grain boundaries will increase the diffusion of oxygen and thereby elevate the oxidation rate. Due to the smaller size of the lithium versus the sodium and potassium ions, it would be easier for lithium to enter the grain boundaries of the dense oxide layer and reach the metal–oxide interface.

The accelerated corrosion in LiOH solution results also in absorption of large quantities of hydrogen by the metal and of hydrides precipitated in the metal at the metal–oxide interface. The accelerated oxidation of zirconium alloys cannot be due solely to the presence of a massive hydride layer, since the oxidation of massive

zirconium hydride resembles the oxidation of zirconium metal, but must require a combined effect of for example interfacial roughness and hydride precipitation [8]. The degradation of the protective oxide layer, found on samples exposed at longer time for LiOH solutions, could not be explained by the high hydride concentration. However, when the protective oxide layer has decreased in thickness and both the oxidation rate and hydrogen pickup is high, the presence of large amount of hydrides makes the situation even worse. The increased hydrogen absorption is due to degradation of the protective oxide barrier layer. The higher oxidation rate in the lithiated water did not result in a higher hydrogen pickup ratio (see Table 2 comparing 200 days water with 73 days lithiated water) before the second transition. Despite the higher hydrogen pickup ratio for Zircaloy-2 the oxidation rate is higher for Zircaloy-4, Fig. 1, clearly showing that hydrogen does not increase the post-transition oxidation. These observations are supported by other investigations, where the corrosion of Zircaloy in LiOH solutions has shown that the hydrogen pickup remains constant [1] and the concentration of the LiOH solution did not influence this value [7]. However, when the protective oxide layer is degraded, the hydrogen pickup will increase.

A decrease in the tin content is known to increase the corrosion resistance [36–38] and normally so also in lithiated environment. However, in this investigation the alloy with the highest tin content (Zry-2:B) has the best corrosion resistance in lithiated water, up to the second transition. However, this is rather an effect of the second-phase particles, which in this alloy (Zry-2:B) are smaller than in the other Zircaloy-2 alloy (Zry-2:A). Furthermore, the total content of second-phase particle formers is 25% lower, see Table 1. The microstructure of the oxide layer (cracks, pores) is influenced by the second-phase particles. A common model for the oxidation is that large compressive stresses are generated in the oxide, due to volume increase ($V_{\text{oxide}} \sim 1.5V_{\text{metal}}$), during oxidation. The oxide grows up to a certain thickness where cracks form in the oxide layer, often associated with the transition. The continued oxidation is controlled by diffusion through the protective oxide layer with fairly constant thickness. More cracks are formed at the outer side of this layer, causing an outer non-protective oxide layer. The second-phase particles will have an effect on the stress distribution in the formed oxide. Lower compressive stress present in the oxide will generate fewer cracks and as a consequence less locations where an up-concentration of the LiOH concentration can occur. The mechanical behaviour of the oxide layer is also dependent on crystallography of the oxide grains. Monoclinic phase is mainly formed during the accelerated oxidation rate in lithiated water. Thus it may be speculated that the mechanical properties of the oxide layer will be degraded, since a growing crack can not be stopped by expending the crack energy on a phase transformation (tetragonal to monoclinic) and a higher fraction of cracks will be found in the oxide layer.

6. Conclusions

Zircaloy-2 and Zircaloy-4 samples were oxidised in an autoclave in pure water and in water with lithium added (70 ppm) in order to evaluate the influence of both the alloy composition and the effect of lithium on the oxidation kinetics. Comparing samples subjected to the same oxidation time and the same environment can outline the effect of different alloy compositions. Using one alloy and comparing samples with similar weight gain, the influence of the environment can be depicted. The correlation between hydrogen absorption kinetics and corrosion kinetics is also investigated. The main results are:

- The hydrogen pickup ratio follows the weight gain, not the oxidation rate, up to the second transition. When the protective oxide layer is degraded the hydrogen pickup ratio increases strongly.
- From the impedance measurements a multi-layer model for the oxide can be proposed. The inner part of the oxide, which may act as a barrier for the oxidation process, is thin for samples exposed to lithiated water.
- There are mainly columnar grains in the oxide layer at the oxide/metal interface. The outer oxide layer have both columnar and equiaxed grains present. The fraction of grain type depends on the oxidation kinetics and the environment. Equiaxed grains are found primarily with cracks present. The density of cracks in the oxide layer correlates with the oxidation rate. A high oxidation rate results in a morphology with equiaxed grains.
- The difference in oxidation kinetics for the investigated materials are associated with the second-phase particle distribution for the materials. The microstructure of the oxide layer depends on the stress distribution in the oxide layer. The mechanical properties of the formed oxide layer depend on second-phase particles distribution and crystallography of the grains.

Based on these observations it is suggested that LiOH effects the oxide by partial dissolution and incorporation of lithium ions in the oxide. Newly formed oxide is probably more hydrous and it is reasonably to assume that the grain boundaries are particularly liable to dissolution. The up-concentration of LiOH within cracks and pores could cause the detrimental levels necessary for dissolution. The incorporation of lithium takes place under circumstances where a dissolution–precipitation process occurs. This is supported by the insensibility in

the pre-transition region, for both the compositions of the alloy and the environment.

Acknowledgements

Financial support from the Swedish Nuclear Power Inspectorate (SKi) is gratefully acknowledged. This work was carried out as a part of the Swedish research programme for the understanding of Zircaloy corrosion and hydriding mechanisms, funded by ABB Atom AB, Barsebäck Kraft AB, OKG AB, and Vattenfall. ABB Atom AB is also gratefully acknowledged for material supply.

References

[1] E. Hillner, J.N. Chirigos, The Effect of Lithium Hydroxide and Related Solutions on the Corrosion Rate of Zircaloy in 680 F Water, Bettis Atomic Power Laboratory, Pittsburgh, PA, Contract AT-11-1-GEN-14, 1962.
[2] Y.H. Jeong, J.H. Baek, S.J. Kim, H.G. Kim, H. Ruhmann, J. Nucl. Mater. 270 (1999) 322.
[3] N. Ramasubramanian, N. Precoanin, V.C. Ling, in: L.F.P.V. Swam, C.M. Eucken (Eds.), Zirconium in the Nuclear Industry: Eighth International Symposium, Vol. ASTM STP 1023, Philadephia, PA, 1989, p. 187.
[4] B. Cox, C. Wu, J. Nucl. Mater. 199 (1993) 272.
[5] B. Cox, M. Ungurela, Y.-M. Wong, C. Wu, in: E.R. Bradley, G.P. Sabol (Eds.), Zirconium in the Nuclear Industry: 11th International Symposium, Vol. ASTM STP 1295, Garmisch-Partenkirchen, Germany, 1996, p. 114.
[6] D. Pêcheur, J. Godlewski, J. Peybernès, L. Fayette, M. Noé, A. Frichet, and O. Kerrec, in: G.P. Sabol, G.D. Moan (Eds.), Zirconium in the Nuclear Industry: 12th International Symposium, Vol. ASTM STP 1354, Toronto, Canada, 2000, p. 793.
[7] R.A. Murgatroyd, J. Winton, J. Nucl. Mater. 23 (1967) 249.
[8] M. Oskarsson, E. Ahlberg, U. Södervall, U. Andersson, K. Pettersson, J. Nucl. Mater. 289 (2001) 315.
[9] F. Garzarolli, H. Seidel, R. Tricot, J.P. Gros, in: C.M. Eucken, A.M. Garde (Eds.), Zirconium in the Nuclear Industry: Ninth International Symposium, Vol. ASTM STP 1132, Kobe, Japan, 1991, p. 395.
[10] E. Hillner, Hydrogen Absorption by Zircaloy-2 During Aqueous Corrosion, Effect of Environment, USAEC Report WAPD-TM-411, 1964.
[11] J.R. Macdonald (Ed.), Impedance Spectroscopy: Emphasizing Solid Materials and Systems, Wiley, New York, 1987.
[12] J. Jacquelin, Electrochim. Acta 39 (1994) 2673.
[13] G. Paasch, K. Micka, P. Gersdorf, Electrochim. Acta 38 (1993) 2653.
[14] E.M. Patrito, R.M. Torresi, E.P.M. Leiva, V.A. Macagno, J. Electrochem. Soc. 137 (1990) 524.
[15] N. Khalil, A. Bowen, J.S. Leach, Electrochim. Acta 33 (1988) 1721.
[16] D. Pêcheur, J. Godlewski, P. Billot, J. Thomazet, in: E.R. Bradley, G.P. Sabol (Eds.), Zirconium in the Nuclear Industry: 11th International Symposium, Vol. ASTM STP 1295, Garmisch-Partenkirchen, Germany, 1996, p. 94.
[17] F. Garzarolli, J. Pohlmeyer, S. Trap-Pretsching, H.G. Weidinger, in: Fundamental Aspects of Corrosion on Zirconium Base Alloys in Water Reactor Enviroments, Vol. IAEA, Technical Committe Meeting, IWGFPT-34, Portland, Ore, USA, 1989, p. 65.
[18] N. Ramasubramaninian, in: C.M. Eucken, A.M. Garde (Eds.), Zirconium in the Nuclear Industry: Ninth International Symposium, Vol. ASTM STP 1132, Kobe, Japan, 1991, p. 613.
[19] R.A. Perkins, R.A. Busch, in: C.M. Eucken, A.M. Garde (Eds.), Zirconium in the Nuclear Industry: Ninth International Symposium, Vol. ASTM STP 1132, Kobe, Japan, 1991, p. 595.
[20] B. Cox, Y.-M. Wong, in: C.M. Eucken, A.M. Garde (Eds.), Zirconium in the Nuclear Industry: Ninth International Symposium, Vol. ASTM STP 1132, Kobe, Japan, 1991, p. 643.
[21] H. Coriou, L. Grall, J. Meunier, M. Pelras, H. Willermoz, J. Nucl. Mater. 7 (1962) 320.
[22] S.G. McDonald, G.P. Sabol, K.D. Sheppard, in: Zirconium in the Nuclear Industry: Sixth International Symposium, Vol. ASTM STP 824, 1984, p. 519.
[23] J.M. Wright, W.T. Lindsey, T.R. Druga, The Behaviour of Electrolytic Solutions at Elevated Temperatures as derived from Conductance Measurements, Bettis Atomic Power Laboratory, Pittsburgh, PA,WAPD-TM-204, 1961.
[24] M. Yoshimura, T. Hiuga, M. Shimada, J. Am. Ceram. Soc. 69 (1986) 583.
[25] M. Oskarsson, E. Ahlberg, K. Pettersson, J. Nucl. Mater., this issue, p. 126.
[26] M. Oskarsson, E. Ahlberg, U. Andersson, and K. Pettersson, J. Nucl. Mater. (2001) (submitted).
[27] C.F. Baes, R.E. Mesmer, The Hydrolysis of Cations, Krieger, 1976.
[28] A.E. Regazzoni, M.A. Blesa, A.J.G. Maroto, J. Colloid Interf. Sci. 91 (1983) 560.
[29] S.M. Ahmed, J. Can. Chem. 44 (1966) 1663.
[30] J.A. Davis, R.O. James, J.O. Leckie, J. Colloid Interf. Sci. 63 (1978).
[31] J.A. Davis, R.O. James, J.O. Leckie, J. Colloid Interf. Sci. 67 (1978) 90.
[32] J.A. Davis, R.O. James, J.O. Leckie, J. Colloid Interf. Sci. 74 (1980) 32.
[33] S. Ardizzone, S. Carella, Electrochim. Acta 36 (1991) 2189.
[34] M. Gunnarsson, A.-M. Jakobsson, S. Ekberg, Y. Albinsson, E. Ahlberg, J. Colloid Interf. Sci. 231 (2000) 326.
[35] A. Cimino, D. Gazzoli, G. Minelli, M. Valigi, J. Mater. Chem. 2 (1992) 75.
[36] M. Harada, M. Kimpara, K. Abe, in: C.M. Eucken, A.M. Garde (Eds.), Zirconium in the Nuclear Industry: Ninth International Symposium, Vol. ASTM STP 1132, Kobe, Japan, 1991, p. 368.
[37] A.M. Garde, S.R. Pati, M.A. Krammen, G.P. Smith, R.K. Endter, in: C.M. Eucken, A.M. Garde (Eds.), Zirconium in the Nuclear Industry: 10th International Symposium, Vol. ASTM STP 1245, Baltimore, MD, 1994, p. 760.
[38] P. Barberis, J. Nucl. Mater. 226 (1995) 34.